Materials Today Communications 26 (2021) 102084

Contents lists available at ScienceDirect

Materials Today Communications

journal homepage: www.elsevier.com/locate/mtcomm

Solar thermal evaporation using bubbly nanofluids with recyclable magnetic particles

Yue Shan [a], Guansheng Yao [a], Jinliang Xu [a,b], Guohua Liu [a,b,*]

[a] Beijing Key Laboratory of Multiphase Flow and Heat Transfer for Low Grade Energy Utilization, North China Electric Power University, Beijing 102206, China
[b] Key Laboratory of Power Station Energy Transfer Conversion and System (North China Electric Power University), Ministry of Education, Beijing 102206, China

ARTICLE INFO

Keywords:
Solar steam
Thermal boundary layer
Recyclable nanofluids
Air bubbles

ABSTRACT

Nanofluids have been extensively studied as light absorption and heat transfer medium for solar energy harvesting. In this work, we, for the first time, investigate the convective bubbly flow in recyclable Fe_3O_4 nanofluids for solar steam generation. The low-cost nanoparticles inherently exhibit broadband light harvesting properties and facile recyclability. The great amount of dispersed bubbles not only work as light transfer center to amplify solar flux, but also provide large areas for mass transport across the interfaces. Our experimental results show that the bubbly nanofluid can significantly enhance the solar thermal evaporation. The coupling effect from light harvesting nanoparticles and dispersed air bubbles finally results in 2.48 times enhancement of the evaporation rate compared to base water. Based on the experimental results, a fully discussion on heat transfer mechanisms around the coupling of nanoparticles and bubbles is additionally provided, in which the thermal boundary layers induced by the particle chain around bubbles played significant roles. This work opens an economic and efficient way for accelerating solar vapor generation, and such concept and methods can be translated into industrial applications such as solar desalination and wastewater treatment.

1. Introduction

Nanofluids are engineered nanoparticle dispersions in a base fluid. Owing to their large specific surface areas, the properties of nanoparticles are dominated by their surfaces rather than the bulk. This endows nanofluids with favorable optical and thermal properties. Various nanofluids have been studied for solar water evaporation (SWE) due to their excellent light harvesting properties [1–3]. By using gold nanoparticles, 78 % photo-thermal conversion efficiency was reached under only the particle concentration of 6 ppm [4]. While plasmonic nanostructures only absorb a small amount of light around their resonance peak [5,6]. To extend the light absorption, carbon-based nanomaterials such as carbon nanotube and graphene oxides are seeded in fluids for solar evaporation [7–9]. The nanofluids achieve above 85 % absorption owing to the full-spectrum absorption ability [10,11]. However, robust dispersion of nanofluids under intensive solar irradiation remains challenging. Some surfactants have been introduced to stabilize nanofluid, yet the negative influence makes it ineligible [12]. Nanofluids with metallic oxides or copper chalcogenide materials is promising alternatives for solar evaporation due to their low cost and low cytotoxicity [13–15]. However, the photo-thermal conversion efficiency of them is sort of unsatisfying. In general, nanofluids can efficiently absorb solar energy as a volumetric heating system, which is an efficient media for solar evaporation [16]. Nevertheless, practical deployment of solar nanofluids is still challenge because of their trend to agglomeration, which leads to a waste of nanomaterials along with secondary pollution to the environment.

In order to realize the sufficient utilization of resources, recyclable magnetic Fe_3O_4 nanoparticles are explored because of their advantages of low-priced, stable, and non-toxic. The magnetic nanoparticles can be prepared by diverse methods, such as hydrothermal together with solvothermal synthesis, microemulsion, co-precipitation and sonochemical hydrolysis, etc [17]. On this basis, Chen R et al. [18] conducted 10 cycles experiment to test the recyclability of Fe_3O_4 nanoparticles and found little reduction in solar-to-vapor performance. Along this line, enhancement ratio of solar-to-vapor performance by nanofluids was studied. For instance, Fe_3O_4@TiO_2 composite nanofluid was confirmed to achieve 1.2 times enhancement in evaporation rate under 1 sun [19], and Fe_3O_4@PDA composite nanofluid was examined to reach 1.69 times enhancement under 1.5 suns [20]. Moreover, some researchers

* Corresponding author at: Beijing Key Laboratory of Multiphase Flow and Heat Transfer for Low Grade Energy Utilization, North China Electric Power University, Beijing 102206, China.
E-mail address: liuguohua126@126.com (G. Liu).

https://doi.org/10.1016/j.mtcomm.2021.102084
Received 15 November 2020; Received in revised form 1 January 2021; Accepted 21 January 2021
Available online 27 January 2021

decorated Fe_3O_4 nanoparticles with carbon-based materials for further improvement of solar absorption. It is found that these composite materials can absorb over 90 % of sunlight, and the evaporation rates can be enhanced by over 2 times than that of base solution [21,22]. Obviously, recyclable magnetic nanomaterials can be used alone or loading on other particles to function as efficient light-absorbers for solar thermal evaporation.

Bubble column evaporator is a mature technology for diverse industries, in which the carrier gas is dispersed into the column to form large amount of small bubbles [23]. The enormous number of bubbles provide large interfacial area to enhance the heat and mass transfer. In our previous study [24], gold nanofluids have been introduced into bubble column to enhance solar vapor generation, achieving a three times enhancement of the evaporation rate under 2 suns. However, gold nanomaterials are too expensive for light absorption, which limits the technology for practical application. In this work, along this line, we for the first time studied the convective bubbly flow in recyclable Fe_3O_4 nanofluids for solar vapor generation. The low-cost magnetic nanoparticles inherently exhibit broadband light harvesting properties and facile recyclability. The bubbles can work as light scattering center to extend the optical pathway and increase light flux. Our experimental results showed that the ferric oxide nanofluid can effectively improve the evaporation rate, and a better performance also can be achieved after injecting the air bubbles.

2. Materials and methods

2.1. Materials preparation

Fe_3O_4 nanoparticles were synthesized referring to the chemical co-precipitation method [17]. First, $FeCl_3{\cdot}6H_2O$ of 82 g and $FeCl_2{\cdot}4H_2O$ of 30 g were dissolved in 2.2 L deionized water (DI water) in a polypropylene container. Second, 190 ml of NH_4OH at a concentration of 29 % was rapidly added to the solution. After 2 min, citric acid monohydrate of 95 g was added. The mixture was then transferred to a glass beaker and ultrasonic for one hour. After the reaction, the Fe_3O_4 nanoparticles were sedimented with magnets for 30 min. After discarding the supernatant and adding 500 ml acetone, simple ultrasound was performed again. In this way, particles can be purified by using magnet once again. This process was repeated three times. The nanoparticles were then dispersed in DI water of 180 ml, forming Fe_3O_4 nanoparticle water/acetone solution of ~250 g. With continuous air flow, acetone was evaporated on a hot plate at 60 °C for two hours. The largest nanoparticles were removed with a magnet for about 10 min.

2.2. Characterization

Fig. 1a shows the transmission electron microscopy (TEM) image of the obtained Fe_3O_4 nanoparicles. As it can be seen, the nanoparticles are basically regular sphere with good dispersion. The nanoparticles were analyzed by Image J software to determine an average diameter about 20 nm. The spacing of particles was successfully maintained at a sufficiently small value (less than particle size), inferring the fluid can sustain good stability. By referring to the previous works [9,20], the Fe_3O_4 nanofluid with a volume fraction of 0.1 %, namely 5.18 g/L, was prepared and used for our experiment. Different from other solar-thermal materials, Fe_3O_4 magnetic nanoparticles can be easily recycled with magnets, as shown in Fig. 1b.

The light absorption properties (*ac*) are measured as shown in Fig. 1c, which are defined as the fractions of light absorbed per unit distance in an absorbing medium [25]. The total diffuse reflectance and transmittance measurements were recorded in a wavelength range of 300−900 nm using UV–vis Spectrophotometer (UV3600). Inverse adding-doubling method is used for the quantitative analysis of the optical properties, which determines the absorption coefficient based on the measured values of the total diffuse reflectance and transmittance [26]. This method validates for the arbitrary ratio of absorption coefficient, making the value of the absorption property become comparable

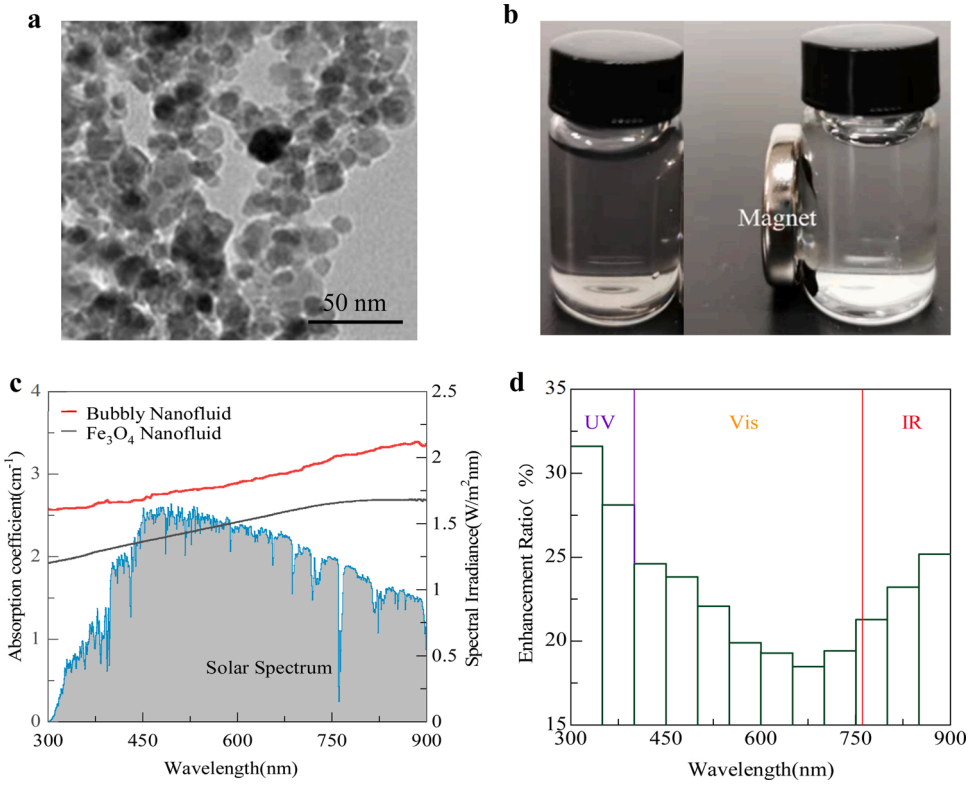

Fig. 1. Characteristics of Fe_3O_4 nanofluids. (a) TEM of the prepared nanoparticles, (b) picture of nanofluid sample and its magnetism, (c) the absorption coefficient of 0.1 % Fe_3O_4 nanofluid and (d) the enhancement ratio between I) bubbly nanofluid and II) Fe_3O_4 nanofluid, which was calculated by (I-II)/II.

[27]. Obviously, Fe_3O_4 nanofluids exhibit full spectral absorbability without distinct absorption peak, and the absorption coefficient slightly increases with wavelength (Fig. 1c). The absorption curve of bubbly nanofluid exhibits small oscillation due to the turbulence of bubbly flow. The average absorption coefficients of 0.1 vol% Fe_3O_4 nanofluid and bubbly nanofluid are 2.39 cm^{-1} and 2.94 cm^{-1}, while the maximum *ac* of them are 2.69 cm^{-1} and 3.39 cm^{-1} respectively in the whole wavelength range of 300−900 nm. The absorptivity (A) can be expressed as: $A = 1 - EXP(-ac)$. In this way, the average absorptivity of 5.18 g/L Fe_3O_4 nanofluid and bubbly nanofluid can be calculated to be 90.87 % and 94.7 % respectively. When comparing the absorption property of bubbly nanofluid with base nanofluid, an enhancement ratio above 20 % can be achieved (Fig. 1d). It is evident that the enhancement ratios are high under ultraviolet and infrared bands, while that of visible wavelength is less. The average enhancement ratios of UV, Vis and NIR bands are 29.864 %, 21.086 % and 23.362 % respectively.

2.3. Experimental procedure

Fig. 2 shows the experiment setup of SWE. The key component is a glass column with 100 mm height and 40 mm inner diameter. A porous metal sinter is embedded into this column to produce bubbles. Air supplied from a gas cylinder flows through the sinter and a valve is used to keep a constant flow rate. By this way, a great amount, small dispersed bubbles can be continuously produced in the glass column filled with fluids. The water surface temperature was monitored by an infrared camera (IR 5300 Series, Germany), meanwhile, the flow patterns was recorded via a high-speed camera (IDT Motion Pro Y4, USA). The incident irradiation comes from a solar simulator (CEL-PE300-3A) with a standard AM1.5 filter. The solar radiation flux was set as 2 kW/m^2. A high-precision electronic balance was utilized to record the mass change. The whole experiments were carried out at controlled conditions with ambient temperature of 20 ℃ and humidity of 33.2 % under atmospheric pressure.

3. Results and discussions

Flow patterns of bubbly water and bubbly nanofluid are shown in Fig. 3. The pictures are selected every 20 ms when the flow pattern was stable. The flow rate was kept at 20 ml/min to avoid other factors such as splashing. One bubble was circled in red to highlight its rising path (Fig. 3), the most bubbles are spiral movement upward, which increases the mass and heat transfer by introducing more turbulent between phases and extending their resident times [28]. Under spiral trajectory, the main resistance for bubble-rising is the pressure difference, which is related to nanofluid viscosity, but fatefully depends on the shape of bubble itself. By ignoring the inner movement of bubbles, the dynamic equation of bubbles can be discribed as [29,30]: $dv/d\tau = \Delta\rho \cdot g/\rho_g - 3\rho_l C_D v/8\rho_g r$ Where τ is the rising time, ρ_g and ρ_l are the densities of gas and fluid respectively, and $\Delta\rho = \rho_l - \rho_g$, g is the gravity, C_D is the drag coefficient determined by Reynolds number : $C_D = 24\left(1 + 0.15\mathrm{Re}^{0.687}\right)/\mathrm{Re}$

Traditional solar vapor generation requires heating the bulk water to a high temperature to trigger evaporation [31]. In contrast, the surface temperature of nanofluids can be far below the saturation temperature, thereby significantly reduce the heat loss to the environment [8,32]. In this experiment, when air bubbles were introduced in nanofluids, this phenomenon became even more apparent. Fig. 4a shows the temperature change of bubbly and pure nanofluid in 60 min. The surface temperatures increased slowly under the continuous solar radiation. The temperature of both cases increased quickly at first and then gradually saturated after 40 min., except that the surface temperature of bubbly nanofluid was evidently low. Fig. 4b shows the surface temperature distribution after an hour. In general, the gas-liquid interface temperature of bubbly and pure Fe_3O_4 nanofluid reached 34.2 and 36.4 OC, respectively. It is thus evident that the introducing of bubbles reduces the temperature. On the one hand, the perturbation of low temperature bubbles decreases the overall temperature of bubbly nanofluid. On the other hand, the latent heat for vaporization comes from the surrounding liquid near bubbles, so the heat can be fast transferred from the solution to the gas-liquid interface due to the high conductivity of nanofluid.

Fig. 5a and b are the mass loss of water evaporation and the evaporation rate with different fluids, respectively. The bubbly nanofluid has the maximum mass of vapor generation of 0.83 g with the highest evaporation rate of 0.594 kg/m^2·h. The steam quality of bubbly water is

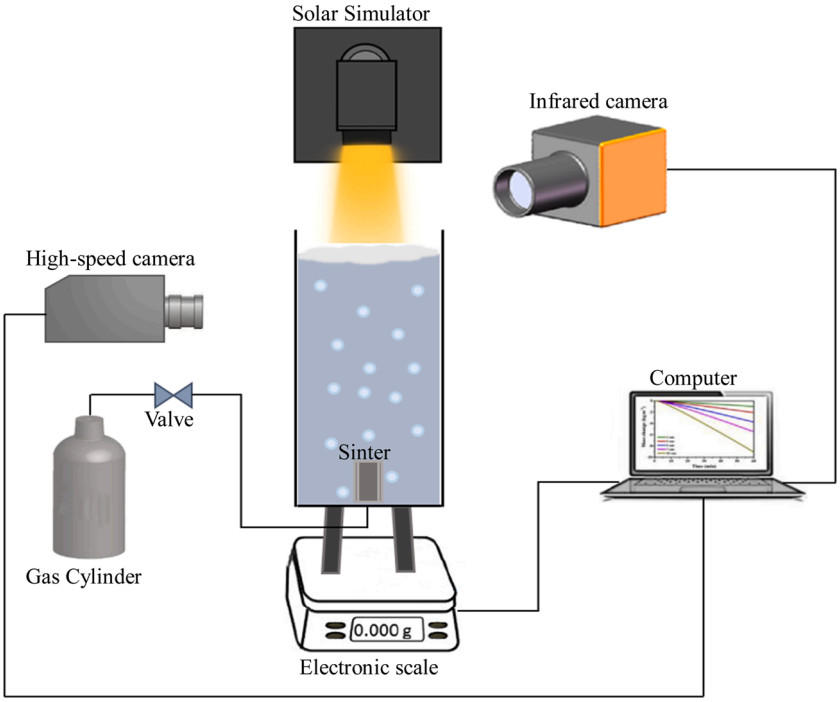

Fig. 2. The diagram of the experiment setup.

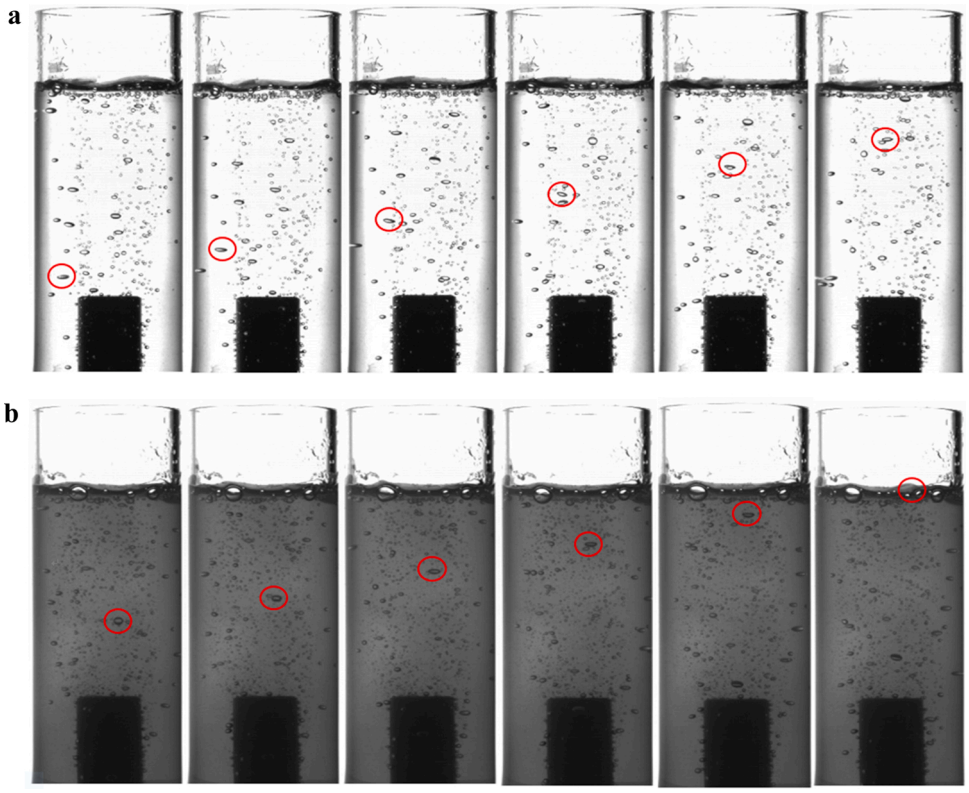

Fig. 3. The typical flow patterns of (a) bubbly water and (b) bubbly nanofluid.

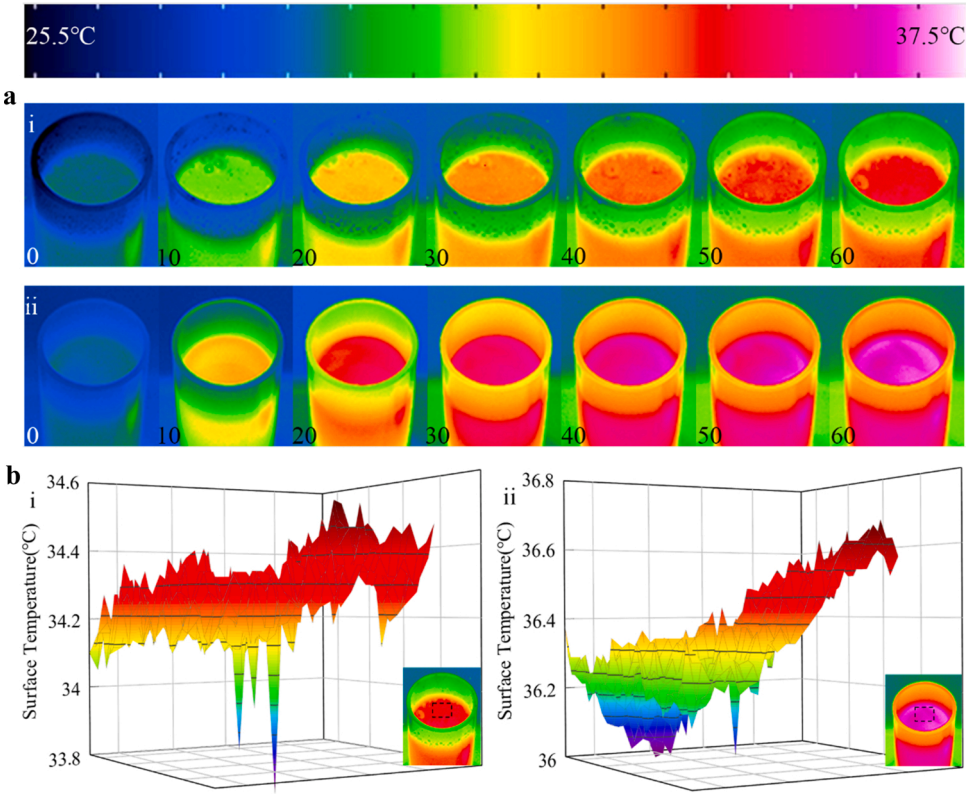

Fig. 4. The temperature evolution in solar evaporation processes. (a) Temperature imagery of i) bubbly nanofluid and ii) Fe_3O_4 nanofluid taken by IR camera in 60 min, (b) the temperature oscillation on the top of the evaporation pond at last minute.

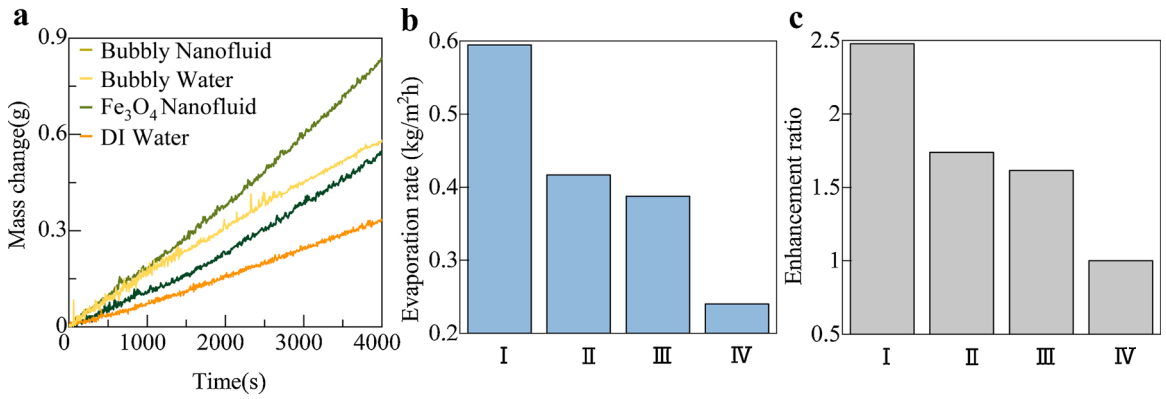

Fig. 5. (a) Mass changes over time with and without bubbly flow nanofluids, (b) the corresponding evaporation rates of I) bubbly nanofluid, II) bubbly water, III) Fe_3O_4 nanofluid and IV) DI water, (c) The enhancement ratios of the evaporation rate compared with base water.

0.582 g and the evaporation rate is 0.416 kg/m^2 h which are higher than those without bubbles, suggesting the injecting bubbles in fluid can significantly promote the SWE process. Fe_3O_4 nanofluid vaporized 0.541 g with an evaporation rate at 0.387 kg/m^2 h slightly less than that of bubbly water, but evidently higher than that of pure water. DI water showed the least vapor generation with mass of 0.335 g, and the slowest evaporation rate of 0.24 kg/m^2 h The enhancement ratio of evaporation is shown in Fig. 6c. The bubbly nanofluid vaporized 2.48 times of steam than that of pure water, which is more than that of simply combination of nanofluid and bubbly water (2.34 times).

The photo-thermal efficiency η_T in Fig. 6a was calculated by the formula $\eta_T = (cm\Delta T + \Delta m h_{fg})/Q_S$ [14], Where c is the specific heat capacity of water (4.2×10^3 J kg^{-1} K^{-1}), m is the total mass of testing fluid (kg), ΔT is the temperature increase of bulk fluid (K), Δm is the weight change of testing fluid (kg), h_{fg} is the phase change enthalpy at 1 atm (2.26×10^6 J·kg^{-1}) and Q_S is the irradiation flux of solar simulator (kW/m^2). Surprisingly, the photo-thermal efficiency of bubbly water (45.4 %) slightly exceeded bubbly nanofluid (43.2 %). This may because of the low bulk temperature of bubbly nanofluid contributes to the reduction of heat exchange with the environment, cutting down heat loss. The photo-thermal efficiency of nanofluid is 41.6 %, slightly lower than bubbly nanofluid. There was no doubt that DI water has the lowest photo-thermal conversion efficiency, namely 27.7 %. The evaporation efficiency in Fig. 6b was calculated by the formula: $\eta = \mathrm{m}\, h_{fg}/Q_S A t$ [9], where Δm is the mass flux of vapor (kg/s), h_{fg} is the latent heat mentioned above, A is the area of the SWE pond (m^2), t is the evaporation time (s) and Q_S is the incoming solar flux (kW m^{-2}). In contrast to the DI water (7.53 %), Fe_3O_4 nanofluid showed a better overall evaporation efficiency of 12.5 %, while the evaporation efficiency of bubbly water was about 13 %. Bubbly nanofluid showed the highest evaporation efficiency of 18.7 %, indicating that the combination of Fe_3O_4 nanoparticles and bubbles maximized the SWE efficiency.

The SWE process in nanofluids can be explained as non-equilibrium thermal evaporation around particles [33]. First of all, nanoparticles absorb solar energy and increase their own temperature, thus quickly heat up surrounding liquid and form nanoscale vapor bubble. These nanobubbles coalesce with others, and eventually rising to the surface where the vapor is released. Then the particles fall back to nanofluids and repeat the SWE process. Another team analyzed the condition to form nanobubbles, and declaim that this occurs only when the surface temperature of nanoparticles exhibiting higher than water spinodal temperature (~550 K), which requires a high intensity of irradiation (>10^5 W/m^2) [34]. In our experiments, the nanobubbles cannot be observed in both cases, however, the injected air bubbles surely play part role of phase-change interfaces even though they were not formed around Fe_3O_4 nanoparticles.

The photo-thermal mechanism around nanoparticles can be fully interpreted as non-radiative relaxation [35]. The optical absorption varies sharply with a wavelength near the bandgap energy, see Fig. 7a. When a particle is illuminated, hole-electron pairs would be generated with energy similar to that of bandgaps. These excited electrons then returned to lower energy level and released energy in the form of non-radiative relaxation phonons, transferring energy to internal holes or surface dangling bonds. Once the energy was released in the form of phonons, the lattice would vibrate to generate heat, which was then diffused outside to heat the surrounding liquid. As the size of particles was much smaller than their distribution distance, the particles can be treated as heating points. The temperature distribution around particle can be described as [36]: $\Delta T(r) = \frac{V_{NP} Q}{4\pi k_0} \frac{1}{r}$. Where $\Delta T(r)$ is the temperature difference between the coordinate point and surroundings, V_{NP} is the

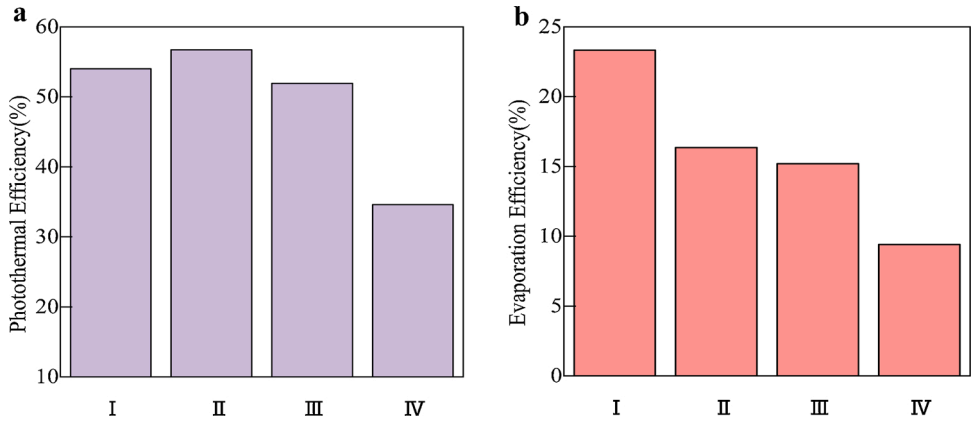

Fig. 6. (a) Photo-thermal efficiency and (b) evaporation efficiency of I) bubbly nanofluid, II) bubbly water, III) Fe_3O_4 nanofluid and IV) DI water.

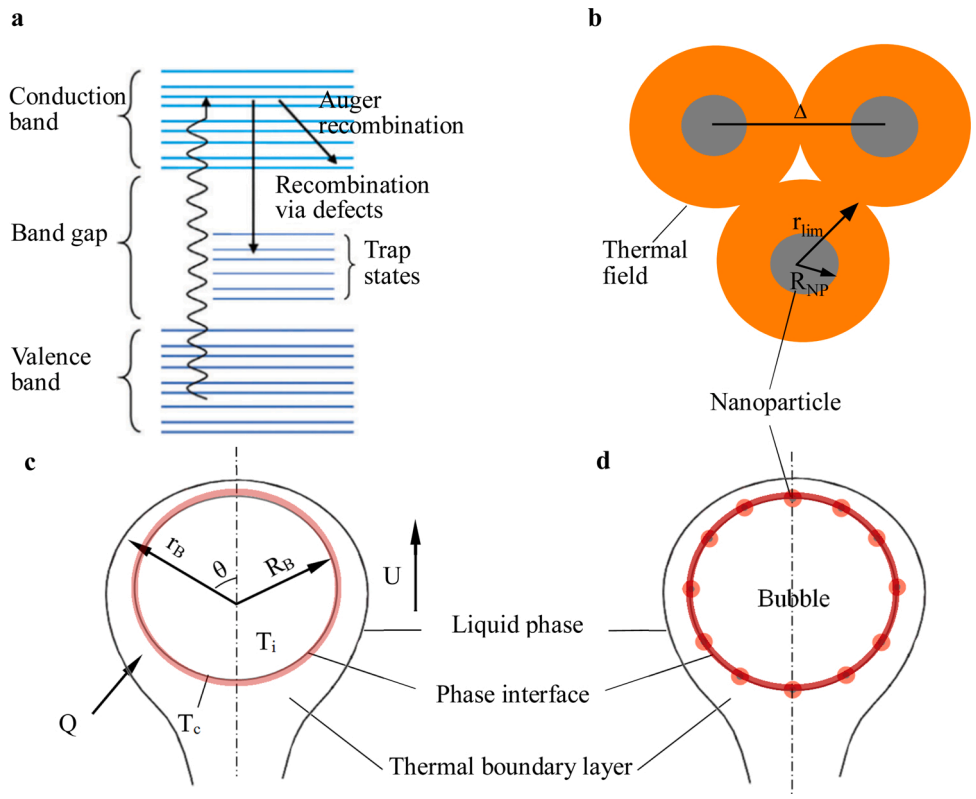

Fig. 7. Heat transfer mechanisms. (a) Photothermic diagram of a Fe_3O_4 nanoparticle, (b) overlapping thermal field of particles. Schematic diagrams of (c) heat transfer process of a bubble in pure water, and (d) the thermal boundary layer around a bubble induced by particle chain.

volume of NF, Q is the heat generated by Fe_3O_4 nanoparticle, k_0 is the thermal conductivity of water, and r is the distance between the coordinate point and the center of particle. Clearly, the temperature around a particle gradually decreases with the spacing distance [37]. Particularly, when the spacing distance between particles was beneath a critical distance r_{lim}, thermal fields of neighboring particles would overlap and result in enhancement of thermal effects [38], see Fig. 7b, and the overall temperature after overlapping can be estimated as [36]: $\Delta T_{tot} \approx \Delta T_{max} \frac{R_{NP}}{\Delta} N_{NP}^{(m-1)/m}$ (m=2 or 3) and $\Delta T_{tot} \approx \Delta T_{max} \frac{R_{NP}}{\Delta} \ln[N_{NP}]$ (m=1) Where ΔT_{max} is the temperature difference between the surface of particle and the surroundings. N_{NP} is the particle numbers, m is the dimension of the particle distribution, and Δ is the average spacing distance.

The self-assembly of nanoparticles around a bubble and their photothermal generation would create a high-temperature thermal boundary around bubble/water interface, which induces intensive mass transport across the interface and fast growing up of the gas bubbles [39]. When air bubbles were introduced in pure water, the latent heat for vaporization merely comes from the surrounding solution (Fig. 7c). In this case, the growth rate can be evaluated by the equation [40–42]: $dR_B/d\tau = Q/\left(4\pi R_B^2 h_{fg} C_\infty\right)$ Where R_B is the radius of bubble, Q is the heat flux, and C_∞ is the gas concentration in bubble. However, the heat generation via high-temperature thermal boundary in bubbly nanofluid is greater than that of pure water. To illustrate this evaporation driven by the high-temperature thermal boundary, a schematic diagram is proposed as in Fig. 7d. By this way, heat production from the nanoparticle chain directly diffuses into the thermal boundary layer around bubble, which directly triggers phase-change evaporation with minimum heat loss, thus improving the SWE efficiency.

4. Conclusions

In this work, we innovatively introduced air bubbles in recyclable Fe_3O_4 nanofluids to promote solar steam generation. Our experimental results show that the bubbly nanofluid can absorb over 94 % of the incident solar flux, and the introduced air bubbles have spiral upward trajectory, which contributes to enhanced heat and mass transfer. Meanwhile, the evaporation temperature of bubbly nanofluid can be distinctly reduced comparing to that without bubbles, which further reduces heat loss to the environment. The bubbly nanofluid thus can significantly improve the evaporation performance with 2.48 times enhancement of the evaporation rate compared to that of base water.

The enhancement might be benefited from the following points: 1) The full spectral absorption property of nanofluid makes sufficient use of solar energy, realizing high efficiency in solar absorption. 2) The spiral trails of bubble movement introduce more turbulent reaction between phases and extend their resident times, which contribute to the enhancement of heat and mass transfer. 3) The nanoparticles directly drive interfacial water evaporation rather than to heat the bulk fluid, thus improve the thermal localization. 4) The broadband light absorption, fast mass transport and intense localized heating of the surrounding liquid finally resulting in the high evaporation rate.

Fully discussions on the heat transfer mechanisms have also been made to disclose the behind mechanisms of the high evaporation performance in bubbly nanofluid. From our perspective, nanoparticles in-situ producing heat around bubble that forms a high-temperature thermal boundary, which gives rise to the intense thermal localization. This work paves a new way using recyclable magnetic nanofluids in bubble column for solar vapor generation, and stands for a basis to develop direct contact evaporators by use of accessible raw materials and renewable energy.

Author declaration

We wish to confirm that there are no known conflicts of interest associated with this publication and there has been no significant financial support for this work that could have influenced its outcome.

We confirm that the manuscript has been read and approved by all named authors and that there are no other persons who satisfied the criteria for authorship but are not listed. We further confirm that the order of authors listed in the manuscript has been approved by all of us.

We confirm that we have given due consideration to the protection of intellectual property associated with this work and that there are no impediments to publication, including the timing of publication, with respect to intellectual property. In so doing we confirm that we have followed the regulations of our institutions concerning intellectual property.

Declaration of Competing Interest

The authors declare no competing financial interests.

Acknowledgements

The authors acknowledge the support from the Nature Science Foundation of China (52076077) and the Fundamental Research Funds for the Central Universities (2020DF002).

References

[1] M. Gao, L. Zhu, C.K. Peh, G.W. Ho, Solar absorber material and system designs for photothermal water vaporization towards clean water and energy production, Energy Environ. Sci. 12 (2019) 841–864.
[2] Y. Pang, J. Zhang, R. Ma, Z. Qu, E. Lee, T. Luo, Solar-thermal water evaporation: a review, ACS Energy Lett. 5 (2020) 437–456.
[3] G. Liu, J. Xu, K. Wang, Solar water evaporation by black photothermal sheets, Nano Energy 41 (2017) 269–284.
[4] H. Zhang, H.J. Chen, X. Du, D. Wen, Photothermal conversion characteristics of gold nanoparticle dispersions, Sol. Energy 100 (2014) 141–147.
[5] S. Wang, K.J. Chen, T.H. Wu, H. Wang, W.Y. Lin, M. Ohashi, P.Y. Chiou, H. R. Tseng, Photothermal effects of supramolecularly assembled gold nanoparticles for the targeted treatment of cancer cells, Angew. Chem. Int. Ed. Engl. 49 (2010) 3777–3781.
[6] X. Yan, G. Liu, J. Xu, S. Wang, Plasmon heating of one-dimensional gold nanoparticle chains, Sol. Energy 173 (2018) 665–674.
[7] Z. Meng, D. Wu, L. Wang, H. Zhu, Q. Li, Carbon nanotube glycol nanofluids: photo-thermal properties, thermal conductivities and rheological behavior, Particuology 10 (2012) 614–618.
[8] T.P. Otanicar, P.E. Phelan, R.S. Prasher, G. Rosengarten, R.A. Taylor, Nanofluid-based direct absorption solar collector, J. Renew. Sustain. Energy 2 (2010), 033102.
[9] X. Wang, G. Ou, N. Wang, H. Wu, Graphene-based recyclable photo-absorbers for high-efficiency seawater desalination, ACS Appl. Mater. Interfaces 8 (2016) 9194–9199.
[10] L. Mercatelli, E. Sani, G. Zaccanti, F. Martelli, P. Di Ninni, S. Barison, C. Pagura, F. Agresti, D. Jafrancesco, Absorption and scattering properties of carbon nanohorn-based nanofluids for direct sunlight absorbers, Nanoscale Res. Lett. 6 (2011) 282.
[11] L. Shi, X. Wang, Y. Hu, Y. He, Y. Yan, Bio-inspired recyclable carbon interface for solar steam generation, J. Bionic Eng. 17 (2020) 315–325.
[12] P.G. Struchalin, E.T. Ulset, P. Kosinski, S.Z. Karazhanov, Y. He, B.V. Balakin, Comparative analysis of photothermal boiling of water enhanced by nano- and micro-particles of carbon black, Mater. Lett. 285 (2021), 129078.
[13] T. Lin, C. Yang, Z. Wang, H. Yin, X. Lu, F. Huang, J. Lin, X. Xie, M. Jiang, Effective nonmetal incorporation in black titania with enhanced solar energy utilization, Energy Environ. Sci. 7 (2014) 967–972.
[14] O.Z. Sharaf, R.A. Taylor, E.A. Nada, On the colloidal and chemical stability of solar nanofluids: from nanoscale interactions to recent advances, Phys. Rep. 867 (2020) 1–84.
[15] S. Wu, D. Zhu, X. Li, H. Li, J. Lei, Thermal energy storage behavior of Al_2O_3-H_2O nanofluids, Thermochim. Acta 483 (2009) 73–77.
[16] J.A. Eastman, S.U.S. Choi, S. Li, W. Yu, L.J. Thompson, Anomalously increased effective thermal conductivities of ethylene glycol-based nanofluids containing copper nanoparticles, Appl. Phys. Lett. 78 (2001) 718–720.
[17] X.M. Li, G. Xu, Y. Liu, T. He, Magnetic Fe_3O_4 nanoparticles_ synthesis and application in water treatment, Nanosci. Nanotech. Asia 1 (2011) 14–24.
[18] R. Chen, Z. Wu, T. Zhang, T. Yu, M. Ye, Magnetically recyclable self-assembled thin films for highly efficient water evaporation by interfacial solar heating, RSC Adv. 7 (2017) 19849–19855.
[19] L. Shi, Y. He, X. Wang, Y. Hu, Recyclable photo-thermal conversion and purification systems via Fe_3O_4@TiO_2 nanoparticles, Energy Convers. Manage. 171 (2018) 272–278.
[20] Q. Wang, Y. Qin, F. Jia, S. Song, Y. Li, Recyclable Fe_3O_4@Polydopamine (PDA) nanofluids for highly efficient solar evaporation, Green Energy Environ. (2020).
[21] L. Shi, Y. He, Y. Huang, B. Jiang, Recyclable Fe_3O_4@CNT nanoparticles for high-efficiency solar vapor generation, Energy Convers. Manage. 149 (2017) 401–408.
[22] Y. Zeng, J. Yao, B.A. Horri, K. Wang, Y. Wu, D. Li, H. Wang, Solar evaporation enhancement using floating light-absorbing magnetic particles, Energy Environ. Sci. 4 (2011) 4074–4078.
[23] Y.T. Shah, B.G. Kelkar, S.P. Godbole, W.D. Deckwer, Design parameters estimations for bubble column reactors, AIChE J. 28 (1982) 353–379.
[24] G. Yao, J. Xu, G. Liu, Solar steam generation enabled by bubbly flow nanofluids, Sol. Energy Mater. Sol. Cells 206 (2020), 110292.
[25] H.G.D. Laszlo, Absorption coefficient, J. Phys. Chem. 32 (2002) 503–506.
[26] S.A. Prahl, Determining the optical properties of turbid mediaby using the adding-doubling method, Appl. Opt. 32 (1993) 559–568.
[27] J.F. Beek, In vitro double-integrating-sphere optical properties of tissues between 630 and 1064 nm, Phys. Med. Biol. 42 (1997) 2255–2261.
[28] M. Taseidifar, M. Shahid, R.M. Pashley, A study of the bubble column evaporator method for improved thermal desalination, Desalination 432 (2018) 97–103.
[29] D.Y. Hsieh, Some analytical aspects of bubble dynamics, J. Basic Eng. 87 (1965) 991–1005.
[30] D. Legendre, J. Borée, J. Magnaudet, Thermal and dynamic evolution of a spherical bubble moving steadily in a superheated or subcooled liquid, Phys. Fluids 10 (1998) 1256–1272.
[31] Y. Tian, C.Y. Zhao, A review of solar collectors and thermal energy storage in solar thermal applications, Appl. Energy 104 (2013) 538–553.
[32] H. Tyagi, P. Phelan, R. Prasher, Predicted efficiency of a low-temperature nanofluid-based direct absorption solar collector, J. Sol. Energy Eng. 131 (2009), 041004.
[33] O. Neumann, A.S. Urban, J. Day, S. Lal, P. Nordlander, N.J. Halas, Solar vapor generation enabled by nanoparticles, ACS Nano 7 (2013) 42–49.
[34] K. Metwally, S. Mensah, G. Baffou, Fluence threshold for photothermal bubble generation using plasmonic nanoparticles, J. Phys. Chem. C 119 (2015) 28586–28596.
[35] Z. Fang, Y.R. Zhen, O. Neumann, A. Polman, F.J. Garcia de Abajo, P. Nordlander, N.J. Halas, Evolution of light-induced vapor generation at a liquid-immersed metallic nanoparticle, Nano Lett. 13 (2013) 1736–1742.
[36] A.O. Govorov, W. Zhang, T. Skeini, H. Richardson, J. Lee, N.A. Kotov, Gold nanoparticle ensembles as heaters and actuators: melting and collective plasmon resonances, Nanoscale Res. Lett. 1 (2006) 84–90.
[37] G. Ni, N. Miljkovic, H. Ghasemi, X. Huang, S.V. Boriskina, C.-T. Lin, J. Wang, Y. Xu, M.M. Rahman, T. Zhang, G. Chen, Volumetric solar heating of nanofluids for direct vapor generation, Nano Energy 17 (2015) 290–301.
[38] P. Keblinski, D.G. Cahill, A. Bodapati, C.R. Sullivan, T.A. Taton, Limits of localized heating by electromagnetically excited nanoparticles, J. Appl. Phys. 100 (2006), 054305.
[39] D.W. Moore, The boundary layer on a spherical gas bubble, J. Fluid Mech. 16 (2006) 161–176.
[40] Q. Wang, J. Gu, Z. Li, W. Yao, Dynamic modeling of bubble growth in vapor-liquid phase change covering a wide range of superheats and pressures, Chem. Eng. Sci. 172 (2017) 169–181.
[41] Y. Hao, Y. Zhang, A. Prosperetti, Mechanics of gas-vapor bubbles, Phys. Rev. Fluids 2 (2017), 034303.
[42] H.S. Lee, H. Merte, Spherical vapor bubble growth in uniformly superheated liquids, Int. J. Heat Mass Trans. 39 (1996) 2427–2447.